catalysts

MDPI

Article

The Contradicting Influences of Silica and Titania Supports on the Properties of Au^0 Nanoparticles as Catalysts for Reductions by Borohydride

Gifty Sara Rolly [1], Alina Sermiagin [1], Krishnamoorthy Sathiyan [1], Dan Meyerstein [1,2,*] and Tomer Zidki [1,*]

[1] Department of Chemical Sciences, The Radical Research and Material Research Centers, Ariel University, Ariel 4077625, Israel
[2] Department of Chemistry, Ben-Gurion University, Beer-Sheva 8410501, Israel
* Correspondence: danm@ariel.ac.il (D.M.); tomerzi@ariel.ac.il (T.Z.); Tel.: +972-54-6002907 (T.Z.)

Abstract: This study investigates the significant impact of metal–support interactions on catalytic reaction mechanisms at the interface of oxide-supported metal nanoparticles. The distinct and contrasting effects of SiO_2 and TiO_2 supports on reaction dynamics using $NaBD_4$ were studied and focused on the relative yields of $[HD]/[H_2]$ and $[D_2]/[H_2]$. The findings show a consistent increase in HD yields with rising $[BD_4^-]$ concentrations. Notably, the sequence of HD yield enhancement follows the order of TiO_2-Au^0-NPs < Au^0-NPs < SiO_2-Au^0-NPs. Conversely, the rate of H_2 evolution during BH_4^- hydrolysis exhibits an inverse trend, with TiO_2-Au^0-NPs outperforming the others, followed by Au^0-NPs and SiO_2-Au^0-NPs, demonstrating the opposing effects exerted by the TiO_2 and SiO_2 supports on the catalytic processes. Further, the catalytic reduction of 4-nitrophenol (4-NP) to 4-aminophenol (4-AP) confirms the catalytic mechanism, with TiO_2-Au^0-NPs demonstrating superior activity. The catalytic activity observed aligns with the order of TiO_2-Au^0-NPs > Au^0-NPs > SiO_2-Au^0-NPs, suggesting that SiO_2 donates electrons to Au^0-NPs, while TiO_2 withdraws them. It is of interest to note that two very different processes, that clearly proceed via different mechanisms, are affected similarly by the supports. This study reveals that the choice of support material influences catalytic activity, impacting overall yield and efficiency. These findings underscore the importance of selecting appropriate support materials for tailored catalytic outcomes.

Keywords: borohydride hydrolysis; strong metal–support interactions; isotopic hydrogen composition; kinetics; $NaBD_4$; silica support; titania support; gold nanoparticles; 4-nitrophenol reduction

Citation: Rolly, G.S.; Sermiagin, A.; Sathiyan, K.; Meyerstein, D.; Zidki, T. The Contradicting Influences of Silica and Titania Supports on the Properties of Au^0 Nanoparticles as Catalysts for Reductions by Borohydride. *Catalysts* **2024**, *14*, 606. https://doi.org/10.3390/catal14090606

Academic Editor: Francesco Mauriello

Received: 17 July 2024
Revised: 2 September 2024
Accepted: 6 September 2024
Published: 9 September 2024

1. Introduction

Due to their unique optical, electronic, and catalytic properties, noble metal nanoparticles (M^0-NPs) are considered an intriguing class of compounds for environmental applications [1]. The direct application of metal nanoparticles is inconvenient due to their high tendency to agglomerate. Thus, metal NPs are often supported onto organic and inorganic supports to prevent agglomeration and particle growth [2]. Organic supports, such as polymers or carbon materials, are frequently used for applications such as catalysis, sensors, and drug delivery due to their biocompatibility, ease of functionalization, and tuneable properties [3]. Inorganic oxide supports such as silica, alumina, and titania are often used for catalytic applications due to their high surface area, mechanical stability, and thermal resistance [4–8]. Inorganic oxides can also be functionalized with various surface groups, such as hydroxyl and amino groups, which can enhance the reactivity of the metal particles and improve their catalytic performance. Moreover, using support materials to anchor or immobilize metal nanoparticles can facilitate their separation and recycling from suspensions by filtration or centrifugation [9].

Metal particles supported on the surface of inorganic oxides have shown strong metal–support interactions [10–13]. Metal oxide supports play essential roles in catalytic reactions

through synergistic interactions with the deposited M^0-NPs, generating new interface phenomena such as electron transfer or shape rearrangement that can influence the activity of the catalysts [14–16]. Most studies on metal–support interactions were performed in a vacuum or a gas-solid interface [17,18]. The study of metal–support interactions in a liquid phase is relevant to many practical applications, such as catalysis and biomedicine [19]. Some studies have shown that the properties of M^0-NPs and their interaction with the support materials can be significantly different in a liquid environment compared to a vacuum or gas-solid interface [20].

Studies suggesting that metal oxides affect the catalytic and physical properties of metal NPs were often associated with the reducibility of the central metal in the metal-oxide supports [21,22]. However, such effects were also reported for irreducible oxides like nano-silica supports. Silver, gold, and platinum NPs supported on silica NPs are poorer catalysts for the hydrogen evolution reaction (HER) initiated by $C(CH_3)_2OH\cdot$ radicals than the unsupported M^0-NPs catalysts [23,24]. An earlier study showed that nano-silica, as the support of Ag^0-NPs, similarly affects their chemical properties above and below the point of zero charge (PZC) of the silica support [25]. However, the silica support does not affect the reaction between $CH_3\cdot$ and Ag^0-NPs [26]. Another study indicated some electron transfer from the SiO_2 to the silver that increases the negative charge on the Ag^0-NPs [27].

Catalytic processes involving borohydride as the reducing agent were chosen for this study as borohydride is known to reduce all oxide/hydroxide covers formed on M^0-nanoparticles that might be formed during the catalytic process [28]. It is commonly assumed that the M^0-NPs catalyze the borohydride hydrolysis reaction (BHR) via hydride transfer from the BH_4^- to the M^0-NPs [29–35]:

$$n\cdot BH_4^- + M^0\text{-NP} + 3n\cdot H_2O \rightarrow n\cdot B(OH)_3 + \left(M^0\text{-NP}\right) - H_{4n}^{4n-}N + 3n\cdot H^+ \quad (1)$$

Reaction (1) is then followed by H_2 evolution via either the Heyrovsky or Tafel mechanisms [34]. Alternatively, the $(M^0\text{-NP})\text{-}H_m^-$ may be oxidized in the presence of an oxidizing agent [28,36–38]. However, recent DFT studies indicate that at least on Ag^0 [39] and Au^0 [40], the BH_4^- hydrolysis proceeds via different mechanisms. For Ag^0, the proposed mechanism is [39]:

$$^*BH_4^- + {}^*H_2O \rightarrow {}^*BH_3(OH)^- + {}^*2H \quad (2)$$

$$^*BH_3(OH)^- + {}^*H_2O \rightarrow {}^*BH_2(OH)_2 + {}^*H_2 \quad (3)$$

$$^*BH_2(OH)^- + {}^*H_2O \rightarrow {}^*BH(OH)_2 + {}^*H + {}^*H_2O + {}^*e^- \quad (4)$$

$$^*BH(OH)_2 + {}^*H + {}^*H_2O + {}^*e^- \rightarrow {}^*BH(OH)_3 + {}^*H_2 \quad (5)$$

$$^*BH(OH)_3^- + {}^*H_2O \rightarrow {}^*B(OH)_4^- + {}^*H_2 \quad (6)$$

According to this mechanism, at most, three adsorbed H atoms are formed during the catalytic BH_4^- hydrolysis.

The experimental results [34] for the catalytic H_2 evolution on Ag^0 agree with reactions (2)–(6). However, the catalytic H_2 evolution results on Au^0 indicate a different mechanism, Reactions (7)–(10) [34,40].

$$^*BH_4^- \rightarrow {}^*BH_3 + {}^*H + {}^*e^- \xrightarrow{H_2O_{(aq)}} {}^*H_3B^-OH_2 + {}^*H + {}^*e^- \rightarrow {}^*BH_3(OH)^- + {}^*H_2 \quad (7)$$

(where * indicates species adsorbed on the surface). Reaction (7) is followed by [40]:

$$^*BH_3(OH)^- + {}^*H_2O \rightarrow {}^*BH_2(OH)_2^- + {}^*2H \quad (8)$$

The latter reaction occurs when no *H atoms are present; in their presence, the reaction occurring is:

$$^{*}BH_3(OH)^{-} + {}^{*}H_2O \rightarrow {}^{*}BH_2(OH)_2^{-} + {}^{*}H_2 \quad (9)$$

This reaction is followed by [40]:

$$^{*}BH_2(OH)_2^{-} \rightarrow {}^{*}BH(OH)_2 + {}^{*}H + {}^{*}e^{-} \quad (10)$$

The $^{*}BH(OH)_2$ thus formed is stable and desorbs from the Au^0-NPs into the solution [40]. Furthermore, not all the adsorbed hydrogen atoms on Au^0-NPs form H_2; these conclusions were experimentally supported [40]. According to this mechanism, only three H· atoms are adsorbed on the Au^0-NPs, and the rest of the H_2 is formed without the involvement of adsorbed hydrogen atoms or hydrides. Furthermore, when H· atoms are adsorbed on Au, Reaction (8) is replaced by Reaction (9) [40]. Hence, H_2 evolution and substrate reduction mechanisms must be reconsidered.

Previously, the BD_4^- hydrolysis in the presence of silica-supported silver nanoparticles (SiO_2-Ag^0-NPs) was studied [27]. The results indicated that the silica support affects the isotopic composition of the product hydrogen gas (H_2, D_2, HD), similar to the effect of increasing the BD_4^- concentration (increasing HD) [34], signifying that some electron transfer from the silica [41] to the silver increases the negative charge on the Ag^0-NPs. Given the new DFT results [39,40], one cannot prove that hydrides are present on the SiO_2-Ag^0-NPs as previously suggested [27]. According to the DFT results, during hydrolysis, the transfer of three H atoms from BH_4^- occurs on the Au^0 surface and one H atom on the Ag^0 surface. Although Ni and Co are more active and cheaper than gold, more information regarding the above reactions is available on Au. As the current work is focused on the support effect, we chose to work with gold NPs. Hence, checking whether gold nanoparticles behave similarly on the "inert" silica and reducible titania supports was interesting. To check whether the effects of the supports observed are general, we decided to study a second model reaction, the reduction of 4-NP, as this reaction definitely proceeds via a different mechanism. We also used the reduction of 4-nitrophenol (4-NP) to 4-aminophenol (4-AP) as a model reaction to draw a more general conclusion about the catalytic role of the support. The 4-NP reduction is a widely studied reaction with essential applications in catalysis and environmental remediation [42,43].

2. Results and Discussion

2.1. Characterizations of Au^0-NPs, SiO_2-Au^0-NPs, and TiO_2-Au^0-NPs

The transmission electron microscopy (TEM) images of gold nanoparticles, silica-supported gold NPs, and titania-supported gold nanoparticles are presented in Figure 1, and their corresponding Energy-dispersive X-ray spectroscopic analysis (EDX) spectra are shown in Figure 2. The average size of bare gold NPs was 4.2 nm, and those of supported gold NPs on silica and titania were 3.5 nm and 3.8 nm, respectively, as obtained from Figure S2. The EDX spectra results in Figure 2 confirmed the presence of Au in Au^0-NPs, Si, O, and Au in SiO_2-Au^0-NPs, and Ti, O, and Au in TiO_2-Au^0-NPs. The Cu and C signals originated from the Cu grid. The Atomic % of each element is provided in Table S1. The UV-visible spectra of the Au^0-NPs, SiO_2-Au^0-NPs, and TiO_2-Au^0-NPs are provided in Figure S1.

Figure 3A represents the Powder X-ray diffraction analysis (PXRD) pattern obtained for bare gold NPs. The peaks at 38.2°, 44.4°, 64.6°, and 77.6° correspond to (111), (200), (220), and (311) planes of the face-centered cubic phase of Au [44]. Figure 3B depicts the PXRD pattern obtained for amorphous SiO_2 and SiO_2-Au^0-NPs (JCPDS: 04-0784). The peak observed at 22° relates to amorphous silica [45], and the (111), (200), (220), and (311) planes of the face-centered cubic phase of Au are also observed [44]. Figure 3C shows the PXRD patterns obtained for bare titania and titania-supported gold nanoparticles. For titania, the diffraction peaks of (101), (004), (200), and (211) correspond to the crystal planes of the anatase phase (JCPDS file 21-1272) [46,47], and the diffraction peak of (121) crystal plane at

30.5°confirms the presence of the brookite phase (JCPDS file 29-1360) [48]. The diffraction peaks at (111), (200), (220), and (311) reflection planes at 2θ = 38.2°, 44.4°, 64.6°, and 77.6° show the presence of the face-centered cubic phase of Au [49]. In addition, for Au^0-NPs and TiO_2-Au^0-NPs, a set of peaks at 2θ = 31.67°, 45.44°, 56.51°, 66.36°, and 75.30° were identified as NaCl (subproduct of the reaction) [50].

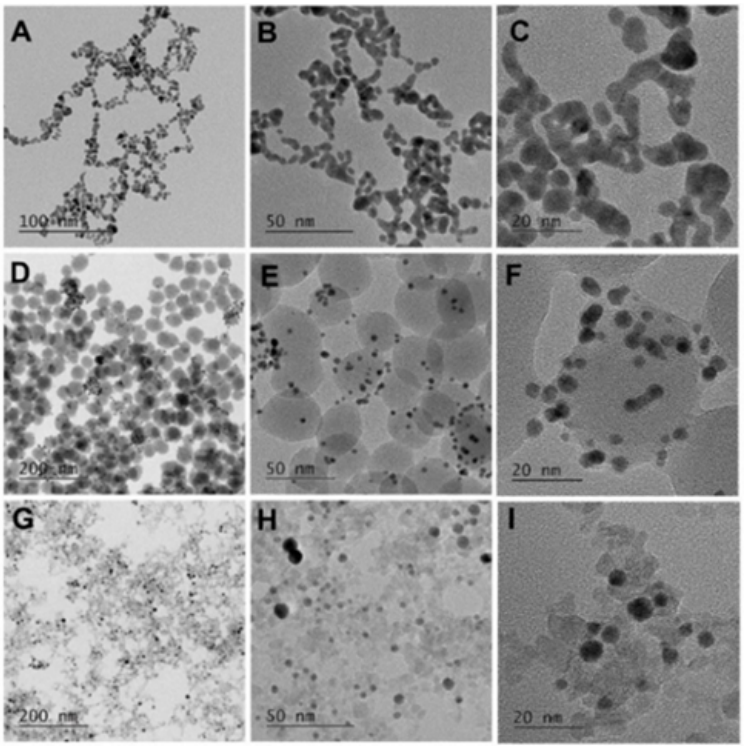

Figure 1. TEM images of (**A**–**C**) Au^0-NPs (4.2 nm), (**D**–**F**) SiO_2-Au^0-NPs (Au^0 = 3.5 nm), and (**G**–**I**) TiO_2-Au^0-NPs (Au^0 = 3.8 nm) at different scales.

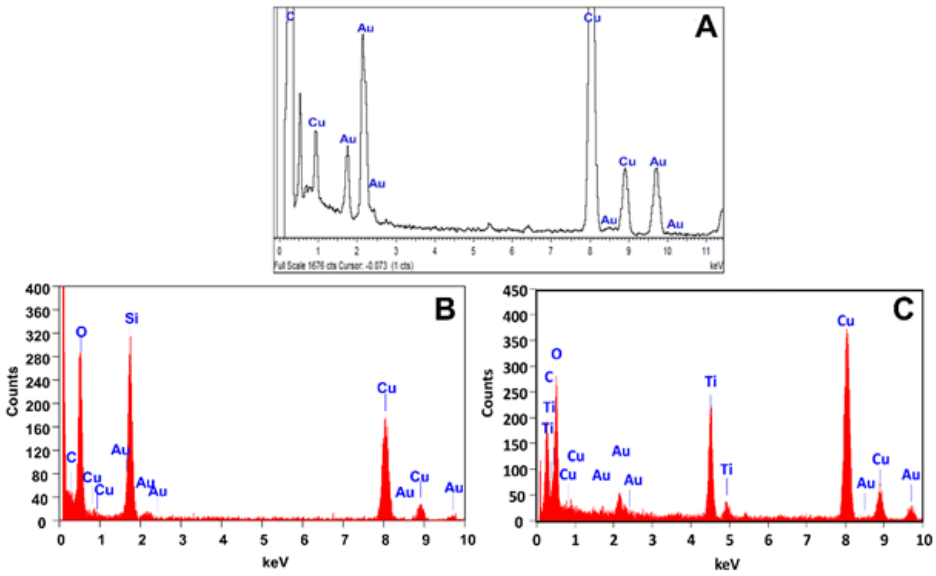

Figure 2. EDX spectra of Au^0-NPs (**A**), SiO_2-Au^0-NPs (**B**), and TiO_2-Au^0-NPs (**C**).

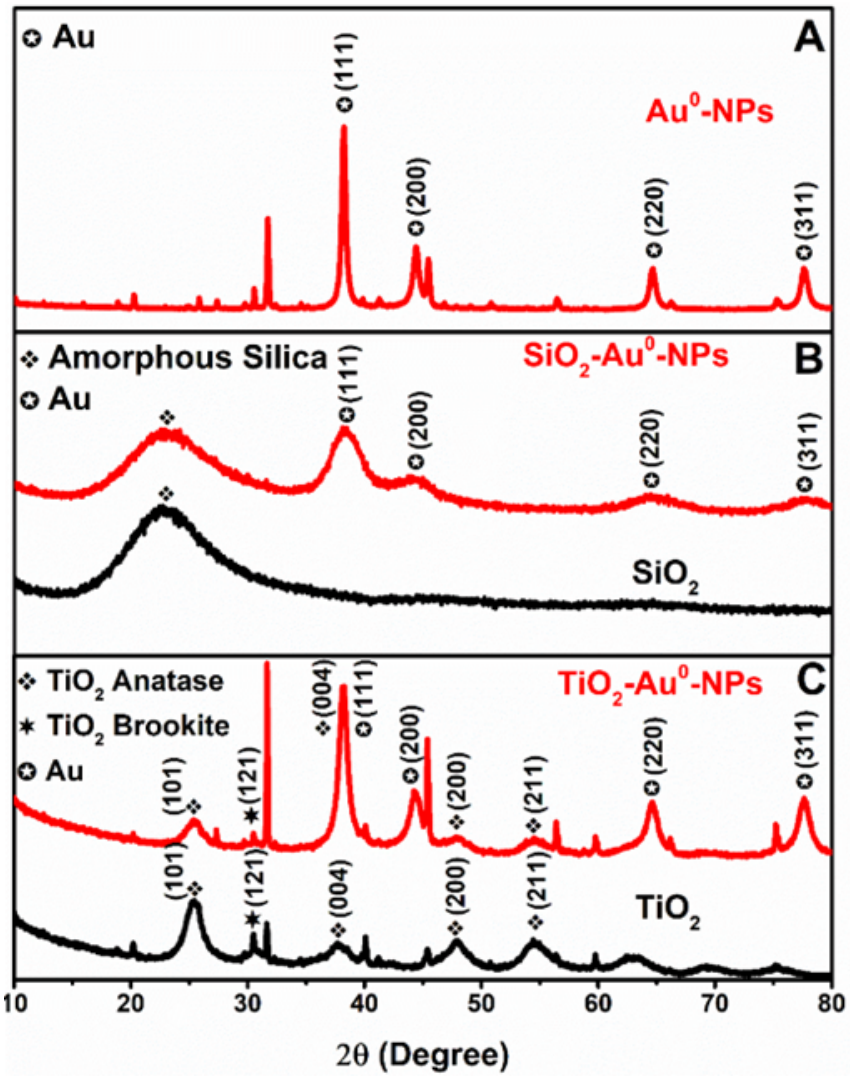

Figure 3. PXRD of Au^0-NPs (**A**), SiO_2-Au^0-NPs and SiO_2 (**B**), and TiO_2-Au^0-NPs and TiO_2 (**C**).

2.2. Isotopic Composition of the Hydrogen Product

Initially, the reactions of SiO_2 (3.5 mM, results from a previous report [27]) and TiO_2 (1.25 mM) with different $NaBD_4$ concentrations were studied as controls. The results are summarized in Table 1. The average hydrogen composition (H_2:HD:D_2) evolved at different [BD_4^-] concentrations for TiO_2 and SiO_2 are 1.0:19.9:0.18 and 1.0:18.0:0.16, respectively. Table 1 demonstrates that the hydrogen formed contains ca. 48% of D atoms in the product in both cases. Note that the borohydride might reduce some $Ti^{IV}O_2$ to $(Ti^{III})_2O_3$ [51].

Later, the reactions were performed in the presence of SiO_2-Au^0-NPs or TiO_2-Au^0-NPs ([Au] = 0.125 mM) and different concentrations of $NaBD_4$; the results are summarized in Table 2 and Figure 4. The SiO_2-Au^0-NP results indicate that the products contained 45.3% D atoms, slightly lower than the blank experiments. However, the kinetic results (Figure 5B) suggest that the reaction occurred at the Au^0 surfaces as the BHR rate increased with [Au^0-NPs]. The TiO_2-Au^0-NP results indicate that the D atoms percentage slightly increases with [BD_4^-]. However, it is considerably lower than expected, meaning a considerable isotopic exchange. This decrease of [D] might be due to a partial, temporary reduction of the titania [51].

Table 1. The hydrogen composition from the reaction of TiO_2-NPs and SiO_2-NPs with BD_4^-.

	$[BD_4^-]$ [mM]	%D	H_2	HD	D_2
TiO_2-NPs	1.0	47.74	1.00	17.64	0.15
	2.0	48.08	1.00	20.35	0.17
	4.0	48.00	1.00	19.47	0.17
	8.0	48.23	1.00	21.36	0.20
	10.0	48.20	1.00	20.80	0.21
SiO_2-NPs [27]	1.0	47.9	1.00	18.7	0.17
	10.0	48.1	1.00	19.9	0.18
	25.0	48.0	1.00	19.5	0.17
	50.0	47.9	1.00	18.7	0.16
	100	46.9	1.00	13.2	0.13

The results of SiO_2-NPs reproduced with permission from reference [27]. The solution pH values were set to 9.0. $[SiO_2] = 3.5 \times 10^{-3}$ M and $[TiO_2] = 1.25 \times 10^{-3}$ M. Each value represents the average of at least five independent experiments. The error limit for the HD:H_2 and D_2:H_2 ratios is ± 2%.

Table 2. The hydrogen composition from the reaction of Au^0, SiO_2-Au^0-NPs, and TiO_2-Au^0-NPs with BD_4^-.

	$[BD_4^-]$ [mM]	%D	H_2	HD	D_2	% HD	% D_2
Au^0-NPs [34]	1.0	41.1	1.0	2.65	0.62	62.06	14.51
	25	45.2	1.0	2.72	0.59	63.10	13.68
	50	46.0	1.0	3.34	0.61	67.47	12.32
	75	46.2	1.0	3.56	0.61	68.85	11.79
	100	45.9	1.0	3.49	0.60	68.56	11.78
SiO_2-Au^0-NPs	1.0	43.3	1.0	3.70	0.34	73.41	6.74
	10	46.2	1.0	5.40	0.48	78.48	6.97
	50	46.2	1.0	5.90	0.45	80.27	6.12
	100	45.6	1.0	5.70	0.39	80.39	5.50
TiO_2-Au^0-NPs	1.0	26.33	1.0	0.93	0.06	46.73	3.01
	10	29.42	1.0	1.08	0.10	49.54	4.58
	50	41.18	1.0	2.64	0.30	67.00	7.61
	75	41.29	1.0	2.5	0.33	65.27	8.62
	100	41.08	1.0	2.33	0.35	63.31	9.51

The results of Au^0-NPs reproduced with permission from reference [34]. The solution pH values were set to 9.0. $[Au] = 1.25 \times 10^{-1}$ mM. Each value represents the average of at least five independent experiments. The error limit for the HD:H_2 and D_2:H_2 ratios is ± 2%.

The results in Figure 4A,C,E indicate that the HD percentage in the hydrogen product increased with $[BD_4^-]$. However, whereas the HD percentage in the hydrogen product formed over SiO_2-Au^0-NPs was substantially higher than that formed over Au^0-NPs, it was significantly lower over TiO_2-Au^0-NPs. Thus, the SiO_2 and TiO_2 supports affect the composition of the hydrogen product differently. This support effect was even more pronounced in the percentage of D_2 in the evolved hydrogen (Figure 4B,D,F), where it decreased with $[BD_4^-]$ over Au^0- and SiO_2-Au^0-NPs, while it increased with $[BD_4^-]$ over TiO_2-Au^0-NPs. These results indicate that the support's nature dramatically affects the borohydride hydrolysis mechanism catalyzed by Au^0-NPs. The observation that $[D_2]$ increased with $[BD_4^-]$ on the TiO_2 support does not fit either mechanism outlined by Reaction (1). A plausible mechanism explaining this observation is described by Reaction (7). Recall the mechanism in Reactions (7)–(10) was proposed on Au [40].

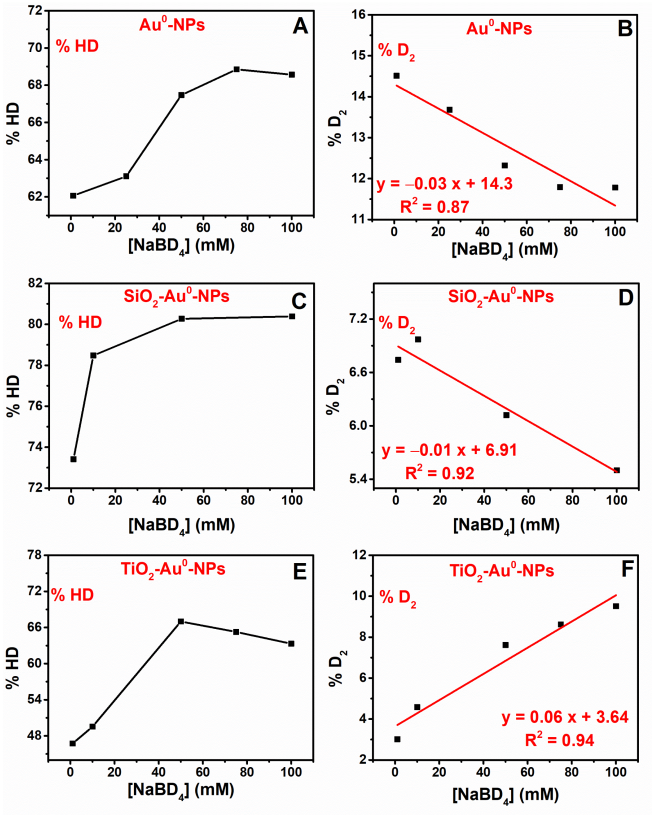

Figure 4. The correlations between %HD and $\%D_2$, as obtained for the $NaBD_4$ reaction with bare Au^0-NPs (**A**,**B**), SiO_2-Au^0-NPs (**C**,**D**), and TiO_2-Au^0-NPs (**E**,**F**).

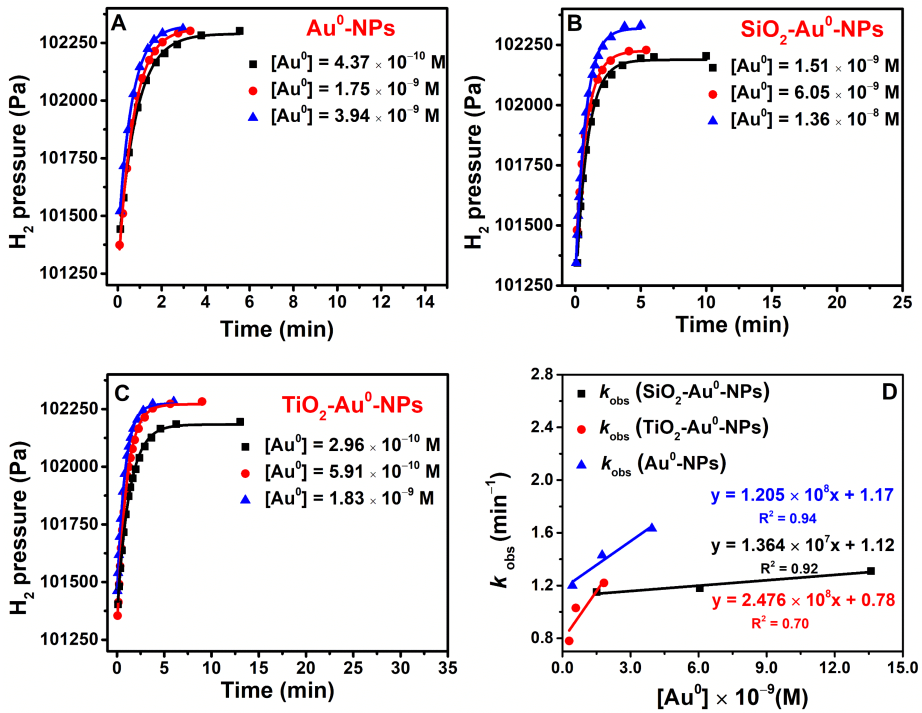

Figure 5. Kinetic plots of hydrogen formation in the hydrolysis of BH_4^- in the presence of Au^0-NPs (**A**), SiO_2-Au^0-NPs (**B**), TiO_2-Au^0-NPs (**C**) at pH 9.0 and the dependence of the observed rate constants on $[Au^0]$ (**D**). $[BH_4^-]$ = 0.50 mM, pH 9.0, the ratios $[Au^0/TiO_2]$ and $[Au^0/SiO_2]$ were constant. Note $[Au^0]$ was the $[Au^{III}]$ used to prepare the NPs, and $[TiO_2]$ was the $[TiCl_4]$ used to prepare NPs.

2.3. Kinetics of the BHR Catalysis over Au^0-, SiO_2-Au^0- and TiO_2-Au^0-NPs

I. The H_2 formation kinetics were studied to answer the questions:

Is the H_2 in the BH_4^- reaction with the SiO_2-Au^0- and TiO_2-Au^0-NPs solely formed at the surface of the Au^0-NPs?

II. Do the supports affect the borohydride hydrolysis rate differently?

The reactions of the gold-based catalysts with BH_4^- were conducted under an argon atmosphere; the rates were measured at different concentrations of Au^0-NPs, SiO_2-Au^0-NPs (constant $[SiO_2]/[Au^0]$), TiO_2-Au^0-NPs (constant $[TiO_2]/[Au^0]$), and TiO_2-NPs (Figure S6). The results are presented in Figure 5A–C, and the computed rate constants are provided in Figures S3–S6. $NaBH_4$ was used for the kinetic study, as the isotope effect usually changes the rate constants of reactions and not their mechanisms; the catalytic trend should be the same as for $NaBD_4$. The lines in Figure 5A–C are the first-order kinetic fits for the experimental data points in these graphs; the observed rate constants are presented in Figure 5D and summarized in Table 3.

Table 3. Observed rate constants of the $NaBH_4$ hydrolysis over various NPs.

Sample	Concentration (M)	Observed Rate Constant k min^{-1}	Rate Constant $k{\cdot}10^7$ M^{-1} min^{-1}
Au^0-NPs	$[Au^0] = 3.94 \times 10^{-9}$	1.63	12
	$[Au^0] = 1.75 \times 10^{-9}$	1.43	
	$[Au^0] = 4.37 \times 10^{-10}$	1.20	
SiO_2-Au^0-NPs	$[Au^0] = 1.36 \times 10^{-8}$, $[SiO_2] = 4.5 \times 10^{-4}$	1.31	1.4
	$[Au^0] = 6.05 \times 10^{-9}$, $[SiO_2] = 2.0 \times 10^{-4}$	1.18	
	$[Au^0] = 1.51 \times 10^{-9}$, $[SiO_2] = 5.0 \times 10^{-5}$	1.15	
TiO_2-Au^0-NPs	$[Au^0] = 1.83 \times 10^{-9}$, $[TiO_2] = 1.00 \times 10^{-5}$	1.22	25
	$[Au^0] = 5.91 \times 10^{-10}$, $[TiO_2] = 5.0 \times 10^{-6}$	1.03	
	$[Au^0] = 2.96 \times 10^{-10}$, $[TiO_2] = 2.50 \times 10^{-6}$	0.78	
TiO_2	1.00×10^{-5}	0.02	
	2.50×10^{-6}	0.02	

The reaction rate increases with [NPs], with the Au^0-NPs having a rate between those of SiO_2-Au^0-NPs and TiO_2-Au^0-NPs. This implies that the H_2 evolution occurs on the Au^0-NPs. As the observed rate constants of supported Au^0-NPs are within an order of magnitude of those of Au^0-NPs, it is reasonable to suppose that all the surface atoms in the NPs are involved. However, it is impossible to rule out that a gold atom in contact with the support has a unique contribution. The catalytic reactions over SiO_2-Au^0-NPs are much faster than over silica blank [27], and the rate constant of H_2 evolution on Au^0-NPs was even faster. On the other hand, the rate constant on TiO_2-Au^0-NPs was twice higher than that on Au^0-NPs. The relatively significant intercepts in Figure 5D suggest equilibria processes. This is tentatively attributed to the BH_4^- adsorption on the Au^0-NPs [40]. The order of BHR catalysis observed is TiO_2-Au^0-NPs > Au^0-NPs > SiO_2-Au^0-NPs. Consequently, the SiO_2 and TiO_2 supports affect the H_2 evolution in opposite directions. The SiO_2 support had a similar effect on increasing BD_4^- concentration, likely due to donating electrons to the Au^0-NPs. On the other hand, the reducible TiO_2 induced a positive charge on the Au^0-NPs. This conclusion aligns with a recent report using a completely different experimental approach [52].

To check whether this support effect also affects other Au^0-NPs-catalyzed reductions, it was decided to study the kinetics of the 4-NP reduction.

UV-visible spectroscopy was employed to monitor the reduction of 4-nitrophenolate ion (λ_{max} = 400 nm) to 4-aminophenol (λ_{max} = 300 nm). The reduction process kinetics were measured every 0.050 min in the presence of SiO_2, TiO_2, TiO_2-Au^0, SiO_2-Au^0, and Au^0 NPs. $NaBH_4$ addition to the catalyst and 4-NP mixture resulted in a gradual decrease of the nitrophenolate peak at 400 nm and a simultaneous formation of the aminophenol peak at 300 nm (Figure 6 and Figure S7), indicating 4-NP conversion to 4-AP. The reduction using blank supports and $NaBH_4$ did not catalyze the reduction process (Figure S7). TiO_2-Au^0-NPs catalyzed 4-NP reduction within 3.5 min after a short induction time, while the reduction was completed within 16 min in the presence of SiO_2-Au^0-NPs after approximately 3 min of induction time. The reduction of 4-NP in the presence of bare Au^0-NPs was completed within 7 min. The kinetic traces of 4-NP reduction monitored at 400 nm are shown in Figure 7. The observed rate constants are 0.66, 0.49, and 0.16 min^{-1} for the catalysis on TiO_2-Au^0-NPs, Au^0-NPs, and SiO_2-Au^0-NPs, respectively. The catalytic activity for 4-NP reduction on Au^0-NPs falls within the range of activities exhibited by titania and silica-supported gold NPs.

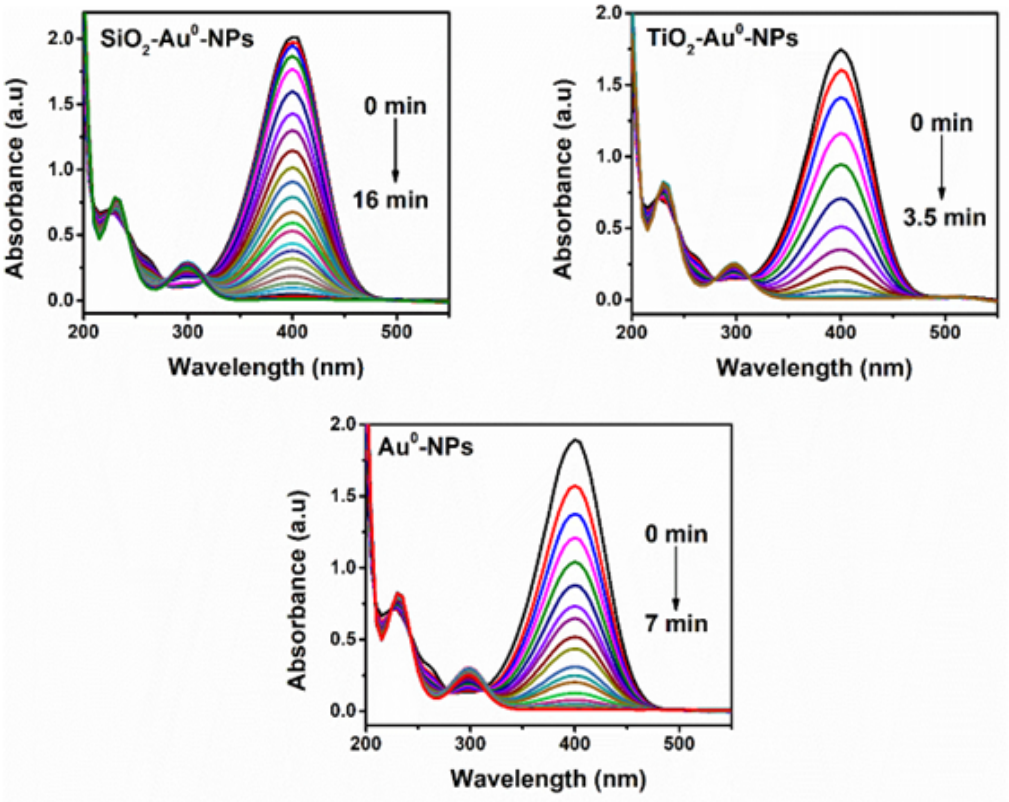

Figure 6. Time-dependent UV-visible spectra of the catalytic reduction of 4-nitrophenol using SiO_2-Au^0-NPs, TiO_2-Au^0-NPs, and bare Au^0-NPs at pH 9.0. The time interval between the cycles was 0.050 min. The concentration of gold was 0.020 mM (in terms of the [Au^{III}] used to prepare the NPs). For better clarity, the absorption spectra shown are at intervals of 0.30 min for TiO_2-Au^0-NPs and 0.70 min for Au^0-NPs and SiO_2-Au^0-NPs.

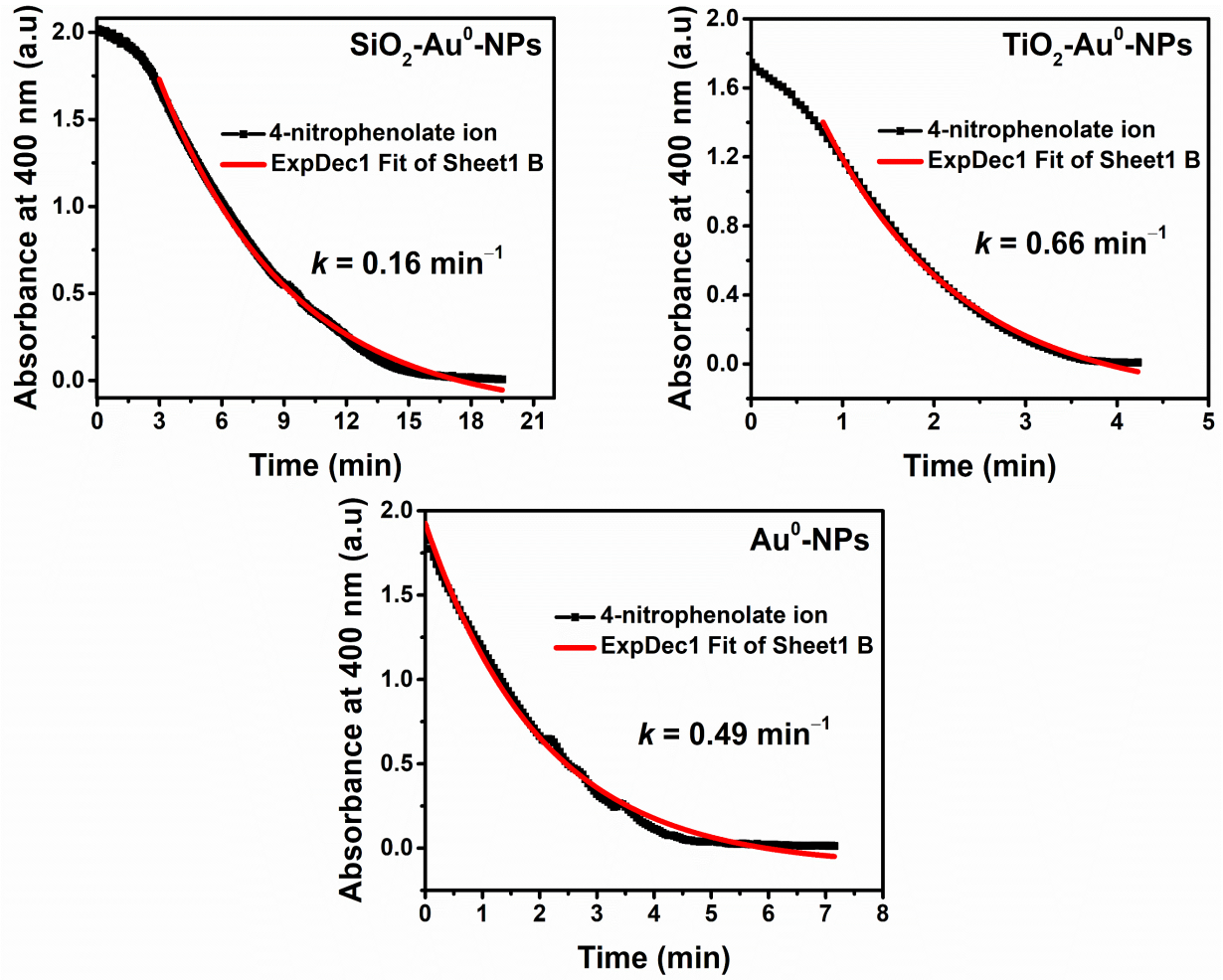

Figure 7. Kinetic traces of 4-NP reduction monitored at 400 nm using SiO_2-Au^0-NPs, TiO_2-Au^0-NPs, and bare Au^0-NPs measured every 0.050 min. The concentration of gold was 0.020 mM (in terms of the [Au^{III}] used to prepare the NPs).

3. Experimental Section

3.1. Synthesis of Au^0-NPs, SiO_2-Au^0-NPs, and TiO_2-Au^0-NPs

All the gold-based catalysts used were previously reported and thoroughly characterized; therefore, the synthesis and characterization are only briefly presented. Gold nanoparticles were prepared by adding an ice-cold solution of $NaBH_4$ to an aqueous solution of $HAuCl_4$ following the well-known Creighton's procedure [53] that was improved by Zidki et al. to obtain more uniform Au^0-NPs [16]. Monodispersed spherical SiO_2-NPs were synthesized using Stöber's method and functionalized with bridging 3-aminopropyltrimethoxysilane (APS) [54]. Colloidal TiO_2 suspensions were prepared by hydrolyzing titanium tetrachloride ($TiCl_4$) as developed by Rabani et al. [55,56]. and later improved by Sathiyan et al. [47]. The obtained SiO_2 and TiO_2 NPs were attached with Au^{III}, followed by $NaBH_4$ reduction to form SiO_2-Au^0-NPs [24] and TiO_2-Au^0-NPs [57]. Detailed synthesis procedures and characterization methods are provided in ESI.

3.2. Reaction of SiO_2-Au^0-NPs and TiO_2-Au^0-NPs with $NaBD_4$

Sealed vials containing argon-saturated SiO_2-Au^0-NPs (pH 9.0) or TiO_2-Au^0-NPs (pH 9.0) suspensions were treated with an equal volume of $NaBD_4$ solution (Ar-saturated). After the reaction of $NaBD_4$ was completed, mass spectrometry (MS, quadruple type gas analyzer, QMG 250 PrismaPro model with electron multiplier by Pfeiffer Vacuum GmbH, Asslar, Germany) gas analysis was performed. Blank reactions were also performed using

bare SiO_2 and TiO_2 nanoparticles. The MS results are summarized in Tables 1 and 2. The tables show the ratios of HD:H_2 and D_2:H_2 at different $NaBD_4$ concentrations.

3.3. Kinetic Measurements

Suspensions of SiO_2-Au^0-NPs, TiO_2-Au^0-NPs, and Au^0-NPs were reacted with an equal volume of $NaBH_4$ solution under Ar at room temperature. The reaction apparatus was connected to an open manometer. The height of the water in the manometer was measured with time to measure the kinetics of the reaction [27]. Different concentrations of SiO_2-Au^0-NPs (pH 9.0), TiO_2-Au^0-NPs (pH 9.0), and Au^0-NPs (pH 9.0), along with their control blanks, SiO_2-NPs, and TiO_2-NPs, were studied with a constant $NaBH_4$ concentration (0.50 mM).

3.4. Catalytic Reduction of 4-Nitrophenol

The 4-nitrophenol (4-NP) reduction to 4-aminophenol (4-AP) was carried out to compare the catalytic efficiency of silica- and titania-supported gold NPs and to assess the support effect on the gold NP activity as schematically presented in Scheme 1. The kinetic studies were performed through straightforward spectroscopic monitoring. A 0.50 mL of the supported gold catalyst (0.125 mM, pH 9.0) was mixed with 1.5 mL of 4-NP (0.20 mM) in a quartz cuvette. A 1.0 mL of freshly prepared $NaBH_4$ solution (10 mM) was added to the mixture, followed by UV-visible spectra recording at specific intervals. The final concentrations were 0.020 mM gold, 0.10 mM 4-NP, and 3.0 mM $NaBH_4$. The molar ratios between [BH_4^-]/[Au], [4-NP]/[Au], [BH_4^-]/[4-NP] were 160, 5, 33. A similar procedure was performed with unsupported Au^0-NPs, silica, and titania. The reaction was monitored by UV-visible spectroscopy in the 200–600 nm wavelength range.

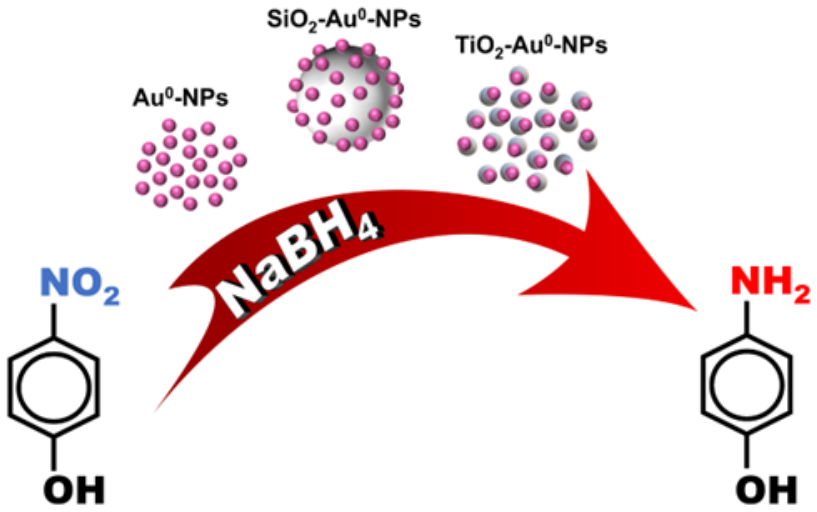

Scheme 1. The catalytic reduction of 4-NP to 4-AP by $NaBH_4$ on Au^0-NPs, SiO_2-Au^0-NPs, and TiO_2-Au^0-NPs catalysts.

4. Conclusions

The findings of this study highlight the significant impact of TiO_2 and SiO_2 supports on the catalytic properties of Au^0-NPs. The results indicate that SiO_2 and TiO_2, as the supports of Au^0-NPs, reversely affect the borohydride hydrolysis kinetics and mechanism. The SiO_2 support, which showed a similar effect to increasing [BD_4^-], likely donates electrons to the Au^0-NPs. Conversely, the reducible TiO_2 induces a positive charge on the Au^0-NPs. These observations are further supported by the results of 4-NP reduction using the same gold catalysts. The catalytic activity of Au^0-NPs for the reduction of 4-NP lies in a range between the activities of titania and silica-supported gold NPs, implying that TiO_2-Au^0-NPs are better catalysts for 4-NP reduction than SiO_2-Au^0-NPs and Au^0-NPs.

Supplementary Materials: The following supporting information can be downloaded at: https://www.mdpi.com/article/10.3390/catal14090606/s1, Figure S1: UV-visible spectra of Au^0-NPs, SiO_2-Au^0-NPs, and TiO_2-Au^0-NPs; Figure S2: Size distribution curves of Au^0-NPs, SiO_2-Au^0-NPs, and TiO_2-Au^0-NPs; Figure S3: Kinetic plots of hydrogen formation in the hydrolysis of BH_4^- in the presence of Au^0-NPs at pH 9.0; Figure S4: Kinetic plots of hydrogen formation in the hydrolysis of BH_4^- in the presence of SiO_2-Au^0-NPs at pH 9.0; Figure S5: Kinetic plots of hydrogen formation in the hydrolysis of BH_4^- in the presence of TiO_2-Au^0-NPs at pH 9.0; Figure S6: Kinetic plots of hydrogen formation in the hydrolysis of BH_4^- in the presence of TiO_2-NPs at pH 9.0; Figure S7: Time-dependent UV-visible spectra of the catalytic reduction of 4-nitrophenol using SiO_2-NPs and TiO_2-NPs, at pH 9.0; Table S1: Atomic % of the elements obtained from EDX.

Author Contributions: Conceptualization, D.M. and T.Z.; Data curation, G.S.R., A.S. and K.S.; Formal analysis, G.S.R.; Funding acquisition, D.M. and T.Z.; Investigation, G.S.R. and A.S.; Methodology, G.S.R., A.S., K.S., D.M. and T.Z.; Project administration, T.Z.; Resources, D.M. and T.Z.; Supervision, D.M. and T.Z.; Validation, D.M. and T.Z.; Visualization, G.S.R.; Writing—original draft preparation, G.S.R.; Writing—review & editing, D.M. and T.Z. All authors have read and agreed to the published version of the manuscript.

Funding: This research was partially funded by the Pazy Foundation grant numbers ID126-2020 and RA1700000176. The APC was waived by the courtesy of MDPI.

Data Availability Statement: The original contributions presented in the study are included in the article/supplementary material, further inquiries can be directed to the corresponding authors.

Acknowledgments: G.S.R. and A.S. thank Ariel University for their Ph.D. scholarships.

Conflicts of Interest: There are no conflicts to declare.

References

1. Lin, Y.; Cao, Y.; Yao, Q.; Chai, O.J.H.; Xie, J. Engineering Noble Metal Nanomaterials for Pollutant Decomposition. *Ind. Eng. Chem. Res.* **2020**, *59*, 20561–20581. [CrossRef]
2. Costa, N.J.S.; Rossi, L.M. Synthesis of Supported Metal Nanoparticle Catalysts Using Ligand Assisted Methods. *Nanoscale.* **2012**, *4*, 5826–5834. [CrossRef] [PubMed]
3. Zhu, Y.; Xu, P.; Zhang, X.; Wu, D. Emerging Porous Organic Polymers for Biomedical Applications. *Chem. Soc. Rev.* **2022**, *51*, 1377–1414. [CrossRef] [PubMed]
4. Jin, Z.; Xiao, M.; Bao, Z.; Wang, P.; Wang, J. A General Approach to Mesoporous Metal Oxide Microspheres Loaded with Noble Metal Nanoparticles. *Angew. Chemie.* **2012**, *124*, 6512–6516. [CrossRef]
5. Ho, J.; Zhu, W.; Wang, H.; Forde, G.M. Mesoporous Silica Spheres from Colloids. *J. Colloid Interface Sci.* **2007**, *308*, 374–380. [CrossRef] [PubMed]
6. Wang, Z.; Feng, J.; Li, X.; Oh, R.; Shi, D.; Akdim, O.; Xia, M.; Zhao, L.; Huang, X.; Zhang, G. Au-Pd Nanoparticles Immobilized on TiO_2 Nanosheet as an Active and Durable Catalyst for Solvent-Free Selective Oxidation of Benzyl Alcohol. *J. Colloid Interface Sci.* **2021**, *588*, 787–794. [CrossRef]
7. Liang, L.; Gu, W.; Jiang, J.; Miao, C.; Krasilin, A.A.; Ouyang, J. Effective CO_2 Methanation over Site-Specified Ruthenium Nanoparticles Loaded on TiO_2/Palygorskite Nanocomposite. *J. Colloid Interface Sci.* **2022**, *623*, 703–709. [CrossRef]
8. Khabra, A.; Cohen, H.; Pinhasi, G.A.; Querol, X.; Córdoba Sola, P.; Zidki, T. Synthesis of a SiO_2/$Co(OH)_2$ Nanocomposite Catalyst for SO_X/NO_X Oxidation in Flue Gas. *Catalysts* **2022**, *13*, 29. [CrossRef]
9. Ndolomingo, M.J.; Bingwa, N.; Meijboom, R. Review of Supported Metal Nanoparticles: Synthesis Methodologies, Advantages and Application as Catalysts. *J. Mater. Sci.* **2020**, *55*, 6195–6241. [CrossRef]
10. Tauster, S.J.; Fung, S.C.; Baker, R.T.K.; Horsley, J.A. Strong Interactions in Supported-Metal Catalysts. *Science* **1981**, *211*, 1121–1125. [CrossRef]
11. Yuan, K.; Guo, Y.; Huang, L.; Zhou, L.; Yin, H.J.; Liu, H.; Yan, C.H.; Zhang, Y.-W. Tunable Electronic Metal–Support Interactions on Ceria-Supported Noble-Metal Nanocatalysts in Controlling the Low-Temperature CO Oxidation Activity. *Inorg. Chem.* **2021**, *60*, 4207–4217. [CrossRef] [PubMed]
12. Chen, Y.; Chen, J.; Zhang, J.; Xue, Y.; Wang, G.; Wang, R. Anchoring Highly Dispersed Pt Electrocatalysts on TiO_x with Strong Metal–Support Interactions via an Oxygen Vacancy-Assisted Strategy as Durable Catalysts for the Oxygen Reduction Reaction. *Inorg. Chem.* **2022**, *61*, 5148–5156. [CrossRef] [PubMed]
13. Shi, Y.; Han, K.; Wang, F. Ni–Cu Alloy Nanoparticles Confined by Physical Encapsulation with SiO_2 and Chemical Metal–Support Interaction with CeO_2 for Methane Dry Reforming. *Inorg. Chem.* **2022**, *61*, 15619–15628. [CrossRef] [PubMed]
14. Lykhach, Y.; Kozlov, S.M.; Skála, T.; Tovt, A.; Stetsovych, V.; Tsud, N.; Dvořák, F.; Johánek, V.; Neitzel, A.; Mysliveček, J.; et al. Counting Electrons on Supported Nanoparticles. *Nat. Mater.* **2016**, *15*, 284–288. [CrossRef]

15. Divins, N.J.; Angurell, I.; Escudero, C.; Perez-Dieste, V.; Llorca, J. Influence of the Support on Surface Rearrangements of Bimetallic Nanoparticles in Real Catalysts. *Science* **2014**, *346*, 620–623. [CrossRef]
16. Zidki, T.; Cohen, H.; Meyerstein, D. Photochemical Induced Growth and Aggregation of Metal Nanoparticles in Diode-Array Spectrophotometer via Excited Dimethyl-Sulfoxide. *Phys. Chem. Chem. Phys.* **2010**, *12*, 12862–12867. [CrossRef]
17. Hernández Mejía, C.; van Deelen, T.W.; de Jong, K.P. Activity Enhancement of Cobalt Catalysts by Tuning Metal-Support Interactions. *Nat. Commun.* **2018**, *9*, 4459. [CrossRef]
18. Saib, A.M.; Gauché, J.L.; Weststrate, C.J.; Gibson, P.; Boshoff, J.H.; Moodley, D.J. Fundamental Science of Cobalt Catalyst Oxidation and Reduction Applied to the Development of a Commercial Fischer–Tropsch Regeneration Process. *Ind. Eng. Chem. Res.* **2014**, *53*, 1816–1824. [CrossRef]
19. Xiang, H.; Feng, W.; Chen, Y. Single-Atom Catalysts in Catalytic Biomedicine. *Adv. Mater.* **2020**, *32*, 1–23. [CrossRef]
20. Zaera, F. Probing Liquid/Solid Interfaces at the Molecular Level. *Chem. Rev.* **2012**, *112*, 2920–2986. [CrossRef]
21. Karim, W.; Spreafico, C.; Kleibert, A.; Gobrecht, J.; Vandevondele, J.; Ekinci, Y.; Van Bokhoven, J.A. Catalyst Support Effects on Hydrogen Spillover. *Nature.* **2017**, *541*, 68–71. [CrossRef] [PubMed]
22. Baron, M.; Bondarehuk, O.; Stacchiola, D.; Shaikhutdinov, S.; Freund, H.J. Interaction of Gold with Cerium Oxide Supports: CeO_2(111) Thin Films vs CeO_x Nanoparticles. *J. Phys. Chem. C.* **2009**, *113*, 6042–6049. [CrossRef]
23. Zidki, T.; Cohen, H.; Meyerstein, D.; Meisel, D. Effect of Silica-Supported Silver Nanoparticles on the Dihydrogen Yields from Irradiated Aqueous Solutions. *J. Phys. Chem. C.* **2007**, *111*, 10461–10466. [CrossRef]
24. Zidki, T.; Bar Ziv, R.; Green, U.; Cohen, H.; Meisel, D.; Meyerstein, D. The Effect of the Nano-Silica Support on the Catalytic Reduction of Water by Gold, Silver and Platinum Nanoparticles—Nanocomposite Reactivity. *Phys. Chem. Chem. Phys.* **2014**, *16*, 15422–15429. [CrossRef]
25. Rolly, G.S.; Meyerstein, D.; Yardeni, G.; Bar-Ziv, R.; Zidki, T. New Insights into HER Catalysis: The Effect of Nano-Silica Support on Catalysis by Silver Nanoparticles. *Phys. Chem. Chem. Phys.* **2020**, *22*, 6401–6405. [CrossRef]
26. Zidki, T.; Hänel, A.; Bar-Ziv, R. Reactions of Methyl Radicals with Silica Supported Silver Nanoparticles in Aqueous Solutions. *Radiat. Phys. Chem.* **2016**, *124*, 41–45. [CrossRef]
27. Rolly, G.S.; Sermiagin, A.; Meyerstein, D.; Zidki, T. Silica Support Affects the Catalytic Hydrogen Evolution by Silver. *Eur. J. Inorg. Chem.* **2021**, *2021*, 3054–3058. [CrossRef]
28. Meistelman, M.; Meyerstein, D.; Bardea, A.; Burg, A.; Shamir, D.; Albo, Y. Reductive Dechlorination of Chloroacetamides with $NaBH_4$ Catalyzed by Zero Valent Iron, ZVI, Nanoparticles in ORMOSIL Matrices Prepared via the Sol-Gel Route. *Catalysts.* **2020**, *10*, 1–17. [CrossRef]
29. Wu, Z.; Mao, X.; Zi, Q.; Zhang, R.; Dou, T.; Yip, A.C.K. Mechanism and Kinetics of Sodium Borohydride Hydrolysis over Crystalline Nickel and Nickel Boride and Amorphous Nickel-Boron Nanoparticles. *J. Power Sources.* **2014**, *268*, 596–603. [CrossRef]
30. Sun, B.; Carnevale, D.; Süss-Fink, G. Selective N-Cycle Hydrogenation of Quinolines with Sodium Borohydride in Aqueous Media Catalyzed by Hectorite-Supported Ruthenium Nanoparticles. *J. Organomet. Chem.* **2016**, *821*, 197–205. [CrossRef]
31. Wang, C.; Astruc, D. Recent Developments of Nanocatalyzed Liquid-Phase Hydrogen Generation. *Chem. Soc. Rev.* **2021**, *50*, 3437–3484. [CrossRef] [PubMed]
32. Ghosh, S.; Kadam, S.R.; Houben, L.; Bar Ziv, R.; Bar-Sadan, M. Nickel Phosphide Catalysts for Hydrogen Generation through Water Reduction, Ammonia-Borane and Borohydride Hydrolysis. *Appl. Mater. Today.* **2020**, *20*, 100693. [CrossRef]
33. Jaleh, B.; Nasrollahzadeh, M.; Nasri, A.; Eslamipanah, M.; Moradi, A.; Nezafat, Z. Biopolymer-Derived (Nano)Catalysts for Hydrogen Evolution via Hydrolysis of Hydrides and Electrochemical and Photocatalytic Techniques: A Review. *Int. J. Biol. Macromol.* **2021**, *182*, 1056–1090. [CrossRef] [PubMed]
34. Sermiagin, A.; Meyerstein, D.; Bar Ziv, R.; Zidki, T. The Chemical Properties of Hydrogen Atoms Adsorbed on M^0-Nanoparticles Suspended in Aqueous Solutions: The Case of Ag^0-NPs and Au^0-NPs Reduced by BD_4^-. *Angew. Chemie Int. Ed.* **2018**, *57*, 16525–16528. [CrossRef]
35. Kang, N.; Djeda, R.; Wang, Q.; Fu, F.; Ruiz, J.; Pozzo, J.; Astruc, D. Efficient "Click"-Dendrimer-Supported Synergistic Bimetallic Nanocatalysis for Hydrogen Evolution by Sodium Borohydride Hydrolysis. *ChemCatChem.* **2019**, *11*, 2341–2349. [CrossRef]
36. Adhikary, J.; Meistelman, M.; Burg, A.; Shamir, D.; Meyerstein, D.; Albo, Y. Reductive Dehalogenation of Monobromo- and Tribromoacetic Acid by Sodium Borohydride Catalyzed by Gold Nanoparticles Entrapped in Sol–Gel Matrices Follows Different Pathways. *Eur. J. Inorg. Chem.* **2017**, *11*, 1510–1515. [CrossRef]
37. Adhikary, J.; Meyerstein, D.; Marks, V.; Meistelman, M.; Gershinsky, G.; Burg, A.; Shamir, D.; Kornweitz, H.; Albo, Y. Sol-Gel Entrapped Au^0- and Ag^0-Nanoparticles Catalyze Reductive de-Halogenation of Halo-Organic Compounds by BH_4^-. *Appl. Catal. B Environ.* **2018**, *239*, 450–462. [CrossRef]
38. Neelam; Meyerstein, D. Zero-Valent Iron Nanoparticles Entrapped in SiO_2 Sol-Gel Matrices: A Catalyst for the Reduction of Several Pollutants. *Catal. Commun.* **2020**, *133*, 105819. [CrossRef]
39. Raju Karimadom, B.; Meyerstein, D.; Kornweitz, H. Calculating the Adsorption Energy of a Charged Adsorbent in a Periodic Metallic System—the Case of BH_4^- Hydrolysis on the Ag(111) Surface. *Phys. Chem. Chem. Phys.* **2021**, *23*, 25667–25678. [CrossRef]
40. Raju Karimadom, B.; Varshney, S.; Zidki, T.; Meyerstein, D.; Kornweitz, H. DFT Study of the BH_4^- Hydrolysis on Au(111) Surface. *ChemPhysChem.* **2022**, *23*, 1–8. [CrossRef]

41. Shin, S.J.; Chung, T.D. Electrochemistry of the Silicon Oxide Dielectric Layer: Principles, Electrochemical Reactions, and Perspectives. *Chem. An Asian J.* **2021**, *16*, 3014–3025. [CrossRef] [PubMed]
42. Pradhan, N.; Pal, A.; Pal, T. Catalytic Reduction of Aromatic Nitro Compounds by Coinage Metal Nanoparticles. *Langmuir.* **2001**, *17*, 1800–1802. [CrossRef]
43. Aditya, T.; Pal, A.; Pal, T. Nitroarene Reduction: A Trusted Model Reaction to Test Nanoparticle Catalysts. *Chem. Commun.* **2015**, *51*, 9410–9431. [CrossRef] [PubMed]
44. Bindhu, M.R.; Umadevi, M. Silver and Gold Nanoparticles for Sensor and Antibacterial Applications. *Spectrochim. Acta Part A Mol. Biomol. Spectrosc.* **2014**, *128*, 37–45. [CrossRef] [PubMed]
45. Bakar, R.A.; Yahya, R.; Gan, S.N. Production of High Purity Amorphous Silica from Rice Husk. *Procedia Chem.* **2016**, *19*, 189–195. [CrossRef]
46. Chenari, H.M.; Seibel, C.; Hauschild, D.; Reinert, F.; Abdollahian, H. Titanium Dioxide Nanoparticles: Synthesis, X-ray Line Analysis and Chemical Composition Study. *Mater. Res.* **2016**, *19*, 1319–1323. [CrossRef]
47. Sathiyan, K.; Bar-Ziv, R.; Mendelson, O.; Zidki, T. Controllable Synthesis of TiO_2 Nanoparticles and Their Photocatalytic Activity in Dye Degradation. *Mater. Res. Bull.* **2020**, *126*, 110842. [CrossRef]
48. Di Paola, A.; Bellardita, M.; Palmisano, L. Brookite, the Least Known TiO_2 Photocatalyst. *Catalysts.* **2013**, *3*, 36–73. [CrossRef]
49. Pol, V.G.; Wildermuth, G.; Felsche, J.; Gedanken, A.; Calderon-Moreno, J. Sonochemical Deposition of Au Nanoparticles on Titania and the Significant Decrease in the Melting Point of Gold. *J. Nanosci. Nanotechnol.* **2005**, *5*, 975–979. [CrossRef]
50. Rojas, J.V.; Castano, C.H. Radiation-Assisted Synthesis of Iridium and Rhodium Nanoparticles Supported on Polyvinylpyrrolidone. *J. Radioanal. Nucl. Chem.* **2014**, *302*, 555–561. [CrossRef]
51. Zhang, X.; Wang, C.; Chen, J.; Zhu, W.; Liao, A.; Li, Y.; Wang, J.; Ma, L. Enhancement of the Field Emission from the TiO_2 Nanotube Arrays by Reducing in a $NaBH_4$ Solution. *ACS Appl. Mater. Interfaces.* **2014**, *6*, 20625–20633. [CrossRef] [PubMed]
52. Ke, W.; Qin, X.; Vazquez, Y.; Lee, I.; Zaera, F. Direct Characterization of Interface Sites in Au/TiO_2 Catalysts Prepared Using Atomic Layer Deposition. *Chem Catal.* **2024**, *4*, 100977. [CrossRef]
53. Creighton, J.A.; Blatchford, C.G.; Albrecht, M.G. Plasma Resonance Enhancement of Raman Scattering by Pyridine Adsorbed on Silver or Gold Sol Particles of Size Comparable to the Excitation Wavelength. *J. Chem. Soc. Faraday Trans. 2 Mol. Chem. Phys.* **1979**, *75*, 790–798. [CrossRef]
54. Stober, W.; Fink, A. Controlled Growth of Monodispersed Silica Spheres in the Micron Size Range. *J. Colloid Interface Sci.* **1968**, *26*, 62–69. [CrossRef]
55. Kasarevic-Popovic, Z.; Behar, D.; Rabani, J. Role of Excess Electrons in TiO_2 Nanoparticles Coated with Pt in Reduction Reactions Studied in Radiolysis of Aqueous Solutions. *J. Phys. Chem. B.* **2004**, *108*, 20291–20295. [CrossRef]
56. Gao, R.; Safrany, A.; Rabani, J. Fundamental Reactions in TiO_2 Nanocrystallite Aqueous Solutions Studied by Pulse Radiolysis. *Radiat. Phys. Chem.* **2002**, *65*, 599–609. [CrossRef]
57. Sathiyan, K.; Bar-Ziv, R.; Marks, V.; Meyerstein, D.; Zidki, T. The Role of Common Alcoholic Sacrificial Agents in Photocatalysis: Is It Always Trivial? *Chem. A Eur. J.* **2021**, *27*, 15936–15943. [CrossRef]